**Modified P3HT materials as hole transport layers for flexible perovskite solar cells**

# Modified P3HT materials as hole transport layers for flexible perovskite solar cells

*Francesca De Rossi[1,†], Giacomo Renno[2,†], Babak Taheri[1], Narges Yaghoobi Nia[1],Viktoria Ilieva[2], Andrea Fin[3], Aldo Di Carlo[1,4], Matteo Bonomo[2,*], Claudia Barolo[2,*], Francesca Brunetti[1,*]*

*[1] CHOSE, Department of Electronic Engineering, Università degli Studi di Roma Tor Vergata, Via del Politecnico 1, 00133 Rome (Italy)*

*[2]Department of Chemistry, Università degli Studi di Torino, Via Pietro Giuria 7, 10125 Turin (Italy)*

*[3] Department of Science and Drug Technology, Università degli Studi di Torino, Via Pietro Giuria 9, 10125 Turin (Italy)*

*[4] CNR-ISM Istituto di Struttura della Materia, via del Fosso del Cavaliere 100, 00133 Rome, Italy.*

## *Abstract*

Flexible perovskite solar cells (f-PSCs) are light-weight, conformal and thus ideal for seamless integration of photovoltaics onto wearable and portable electronics. Nevertheless, the spread of f-PSCs is limited by both the lower efficiency compared to rigid counterparts and the employment of costly materials. Among them, hole-transporting materials (HTM) represent the most expensive component and also a weak spot for long-term stability, due to poor resistance against heat and moisture. Here, we propose poly-3-hexylthiophene (P3HT)-modified HTMs embodying benzothiadiazole (BDT) moieties as electron-poor host. BDT is inserted along P3HT backbone, creating a donor-acceptor system able to promote the charge mobility throughout the HTM. A first series of copolymers, synthetized by Stille coupling, shows a decrease of benzothiadiazole/thiophene ratio (1:2, 1:4, 1:6), allowing to modulate both electronic and optical properties. Additionally, a greener approach (Kumada polycondensation) is employed to synthetize a homologous copolymer (VI-LM-027) embodying a lower amount of BDT that, used as HTM in f-PSCs, leads to power conversion efficiency comparable to commercially available P3HT and shows improved stability under continuous illumination. Finally, VI-LM-027 is also employed in 6x6 $cm^2$ modules, delivering 6.9% efficiency on 16 $cm^2$ of active area and demonstrating the feasibility of the proposed HTMs for large area manufacture.

## *Keywords*

*Perovskite Solar Cells; Hole Transporting Material; Polymers; P3HT; Module; Stability*

## 1. Introduction

The efficiency of flexible perovskite solar cells (f-PSCs) has recently reached up to 19.5% [1], employing a triple cation perovskite layer sandwiched between a tin oxide electron transport layer (ETL) and a spiro-OMeTAD hole transport layer (HTM) in a planar n-i-p architecture. Although still lagging behind their rigid counterparts, which in very short time have rocketed 25.2% efficiency [2], f-PSCs present several appealing features, such as bendability, conformability and high power-to-weight ratio [3], that make them good candidates for several applications, from consumer electronics to avionics and spacecrafts [4]. Flexible substrates require low temperature processes and allow for high throughput roll-to-roll manufacture, which could potentially reduce further fabrication costs and levelized cost of energy (LCOE) [4]. Record efficiencies for lab-scale f-PSCs are still tied to the use of costly materials, such as spiro-OMeTAD: although very efficient as HTM, it needs hygroscopic dopants and is thushighly sensible to moisture [5,6];it is also prone to crystallization and the growth of large crystalline domains can affect the contact between perovskite and HTM at the interface, leading to degradation at elevated temperatures [7,8]; additionally, even though large area deposition has been demonstrated [9], the reduced wettability makes the deposition process complex and incompatible with some large area deposition technique such as slot-die coating [8,10].

To overcome these issues, some organic polymers (e.g. PTAA, PEDOT:PSS, P3HT) have been proposed as hole transport materials (HTM) in PSCs [11–13]. Among them, poly-(3-hexyl-thiophene) (P3HT) [14,15] has been deeply investigated due to its high hole mobility (0.1 $cm^2$ $V^{-1}$ $s^{-1}$) and relatively easy synthesis, that translates into lower production costs [16]. Furthermore, P3HT has demonstrated higher stability compared to the more efficient spiro-

OMeTAD [17,18], thanks to its tolerance to temperatures between -80 °C and 100 °C [19], low permeability to oxygen and strong hydrophobicity [16,20].

P3HT has been successfully used in mesoporous PSCs on rigid substrates, leading to power conversion efficiency (PCE) of 22.7% when employing a wide-bandgap halide perovskite on top of the narrow-bandgap perovskite layer [6]; suitability for large area fabrication has been demonstrated and led to modules delivering 13.3% PCE on 43 $cm^2$of active area (19.25% on small area); also, a very high open circuit voltage ($V_{OC}$) of 1.14 V has been reached by combining three dopants, namely Li-TFSI, TBP, and Co(III)-TFSI [21]. Efficiency as high as 17.49% has been achieved using $Zn(C_6F_5)_2$-doped P3HT in glass-based planar devices [22]. Finally, P3HT has been employed also on flexible substrates, delivering 11.84% PCE in n-i-p devices with cobalt-doped P3HT, and demonstrating mechanical stability up to 600 bending cycles [23].

From a chemical point of view, P3HT belongs to the family of polythiophenes, a group of polymeric materials based on the electron-rich thiophene monomer and known for their remarkable electronic and electrochemical properties. Their dramatic insolubility can be overcome introducing alkyl chains on the thiophene ring, *e.g.* a hexyl group on the 3-position on the thiophene for the P3HT.The presence of lateral chains assures solubility and good processability of the polymer but, making the monomer not symmetric, it could give rise to different regioisomers [24]. High regioregularity (RR) of Head-to-Tail coupling allows to obtain a planar conformation of the polymer, characterized by an extended $\pi$ conjugation and the organization in large crystalline domains. One should notice that P3HTs feature a relatively low stability toward oxidation and could undergo degradation if exposed to UV radiation [25]. Nevertheless, both phenomena are downsized when the polymer is embedded in a complete device, as the UV radiation is filtered by both the glass (or PET in case of flexible devices) and

the active layer and the polymer itself is protected from oxygen contamination by the back-electrode.

Synthesized P3HT usually suffers from insufficient charge transport properties. Therefore, a common approach consists in the modification of the polymer by the addition of dopants, such as $Zn(C_6F_5)_2$ [22], carbon nanotubes (CNT) [26], 2,3,5,6-tetrafluoro-7,7,8,8-tetracyanoquinodimethane (F4TCNQ) [27], cobalt-based salts [21,23], 4-tert-butylpyridine (TBP) [28], lithium bis(trifluoromethanesulfonyl)imide (LiTFSi) [21,28].The latter leads to a better crystallinity of the deposited film and a closer packing of the lateral chains, improving the hole transport throughout the film [29]. Yet, dopants can limit the polymer stability, due to the light-induced generation of radicals and, more importantly, cause ion migration throughout the PSK film [30].

In order to further ameliorate both the charge transport properties and the light stability of P3HT, a feasible approach consists in the insertion (within the polymer chain) of electron-poor moieties leading to the formation of donor-acceptor (D-A) co-polymers. The establishment of D-A couples leads to more effective intramolecular interactions that promote the hole transport [31]. This approach was explored by El-Shehawy et al. [29] who synthesized 2,1,3-Benzothiadiazole (BTD)/P3HT co-polymers, investigating the effect of BTD/3-hexylthiophene (HT) ratio, the position of hexyl chain on the polymers opto-electronic properties and their photovoltaic features in fully organic solar cells. From an energetic point of view, the insertion of a host unit within the P3HT chain allows to finely tune the frontier molecular orbitals (HOMO and LUMO) and, thus, the band gap of the polymer. This approach could be also effectively coupled with the doping of the polymer.

In this work, we report on the synthesis of a series of BDT/P3HT co-polymers aiming at highly soluble (processable) and thermally stable polymers that could lead to improved

photoconversion efficiency and stability once implemented as HTM in PSCs. Two different synthetic approaches are presented: a first group of polymers was obtained by inserting different quantities of BTD moiety into the 3-hexylthiophene backbone to evaluate the BTD effects on the optical and thermal features of the system. As a result, a novel polymer was synthesized by Stille coupling in addition to other two structures, already reported by El-Shehawy and co-workers [29]. Then, a greener synthetic approach based on Kumada polycondensation replaced Stille coupling as polymerization method [32]. Within this approach we chose to introduce a very low amount of BDT, and albeit the information about the exact BDT/HT ratio was lost, better results were achieved with this second strategy in terms of molecular weight, a crucial parameters for cells performance [33,34].

The synthesized D-A polymers were characterised thoroughly and eventually used in f-PSCs as HTMs: they achieved higher operational stability under illumination compared to spiro-OMeTAD and commercially available P3HTs, and efficiency as high as 10.8% on small cells (0.09 $cm^2$) and over 6% on a flexible module with 16 $cm^2$ active area.

## 2. Material and Methods

### 2.1 Materials

Concerning the synthetic part, 5,5'-dibromo-3,3'-dihexyl-2,2'-bithiophene (**7**) and 3-hexylthiophene-2-boronic acid pinacol ester were purchased by TCI Chemicals. 2,1,3-Benzothiadiazole (**1)**, lithium chloride (solution in anhydrous THF) and buthyl lithium were purchased by Sigma Aldrich. Intermediates **2**, **4**, **5**, **6** and copolymers **GRe-2-12** and **GRe-2-14** as hole transport materials were prepared following previously reported procedures[29,49].

Tin (IV) oxide ($SnO_2$) colloidal dispersion in $H_2O$ (15wt%) was purchased from Alfa Aesar. Lead iodide ($PbI_2$) and lead bromide ($PbBr_2$) were purchased from TCI Chemicals;

formamidinium iodide (FAI) and methylammonium bromide (MABr) from Greatcell Solar; Spiro-OMeTAD (99.5%) from Borun; 4-tert-Butylpyridine (TBP), bis(trifluoromethylsulfonyl)imide lithium salt (Li-TFSI), cobalt (III) tris(bis(trifluoromethylsulfonyl)imide) (FK-209), isopropanol (IPA), N-N dimethylformamide (DMF), dimethyl sulfoxide (DMSO) chlorobenzene (CB, 99.9%), acetonitrile from Sigma-Aldrich; P3HT at different molecular weight were supplied by Solaris Chem.

**2.2 Synthesis of modified P3HTs as HTM**

***4,7-dibromobenzo[c][1,2,5]thiadiazole (2)***[49]**.** 2,1,3-Benzothiadiazole **1** (0.51 g, 3.7 mmol, 1 eq.) and N-bromosuccinimide (1.39 g, 7.8 mmol, 2.1 eq.) were dissolved into 5 MlOf $H_2SO_4$. The orange mixture was stirred under heating at 60°C for 3h. After having been cooled at room temperature, the reaction mixture was put into an ice-bath and distilled water (25 mL) was added dropwise. The product was extracted with toluene, the combined organic layers were dried with $Na_2SO_4$ and the solvent was removed in vacuo. The product **2** afforded as a white solid. Yield: 68 %. $^1$H-NMR: (600 MHz, Acetone-d6, ppm) δ: 7.93 (s, 2H).

***4,7-bis(3-hexylthiophen-2-yl)benzo[c][1,2,5]thiadiazole (4)***[29]**. 2** (0.1 g, 0.34 mmol, 1 eq.), 2-(3-hexylthiophen-2-yl)-4,4,5,5-tetramethyl-1,3,2-dioxaborolane **3** (0.25 g, 0.86 mmol, 2.5 eq) and a solution of $K_2CO_3$ (2 M, 3 mL) were dissolved in 4 mL of toluene in a round-bottom flask. $Pd(PPh_3)_4$ (0.05 g) was added and the mixture was deoxygenated with argon for few minutes. The reaction mixture was stirred under heating (100°C) overnight. Then, the mixture was extracted by toluene and the combined organic layers were re-washed with distilled water. The organic phase was dried with $Na_2SO_4$ and the solvent was removed in vacuo. The crude product was purified by chromatography (gradient petroleum ether/ethyl acetate from 100:0 to 90:10), affording **4** as an orange oil. Yield: 94%. $^1$H-NMR (200 MHz, Acetone – d6,

ppm) δ: 7.79 (s, 2H), 7.60-7.57 (d, J = 6 Hz, 2H), 7.18-7.15 (d, J = 6 Hz, 2H), 2.69 (t, J = 8 Hz, 4H), 1.58 (m, 4H), 1.32 – 1.15 (m, 12H), 0.77 (m, 6H).

***4,7-bis(5-bromo-3-hexylthiophen-2-yl)benzo[c][1,2,5]thiadiazole (5)***[29]**.** To a solution of **4** (0.15 g, 0.33 mmol, 1 eq.) in dry THF (5.5 mL) at 0°C, N-bromosuccinimide (0.15 g, 0.81 mmol, 2.6 eq.) was added. After having been stirred for 0.5 h, the mixture was allowed to warm up to room temperature and stirred overnight. The mixture was quenched with saturated aqueous $NH_4Cl$ and the aqueous phase was washed with ethyl acetate. The combined organic layers are dried with $Na_2SO_4$ and the solvent is removed *in vacuo*. The crude mixture is purified by chromatography (gradient petroleum ether/ethyl acetate from 97:3 to 90:10) to generate **5** as a red oil. Yield: 82%. $^1$H-NMR (200 MHz, CDCl3-d, ppm) δ:7.60 (s, 2H), 7.06 (s, 2H), 2.65-2.57 (t, J = 8.1 Hz, 4H), 1.58 (m, 4H), 1.22-1.20 (m, 12H), 0.84-0.78 (m, 6H). TLC: $R_f$=0.5 (EP/EtOAc, 98:2)

***4,7-bis(5-(tributylstannyl)thiophen-2-yl)benzo[c][1,2,5]thiadiazole (6)***[29]**.** Under argon atmosphere, **4** (0.074 g, 0.16 mmol, 1 eq.) was dissolved in dry THF (4 mL) at -78°C. Butyl lithium (0.051 g, 0.791 mmol, 5 eq.) was added dropwise and the mixture was stirred at -78°C. After 1 h, tributyltin chloride (0.31 mL, 1,11 mmol, 7 eq.) was added and the reaction mixture was allowed to warm up at room temperature and stirred overnight. Ethyl acetate was added to the reaction mixture and quenched with $NH_4Cl$ saturated aqueous solution. The aqueous phase was washed several times with ethyl acetate. The combined organic layers were dried with $Na_2SO_4$ and the solvent was removed *in vacuo*. The absence of starting material and mono-substituted compound was checked by TLC. The product **6** was carried forward to the next step without further purifications. TLC: $R_f$ =0.93 (petroleum ether/ethyl acetate 90:10).

***VI-LM-027.***In a Schlenk flask, **5** (0.4 g, 0.63 mmol) was mixed with lithium chloride (0.5 M in THF, 1.40 mL, 0.7 mmol) and *i*PrMgCl (2 M in THF, 0.35 mL, 0.7 mmol) in dry THF (1.5 mL)

under Argon atmosphere. The mixture was stirred at room temperature for 2 hours. Similarly,compound **9** (4.5 g, 12.1 mmol) was mixed with lithium chloride (0.5 M in THF, 26.5 mL, 13.3 mmol), dry THF (65 mL) and *i*PrMgCl (2 M in THF, 6 mL, 12.1 mmol)[39]. The mixture was stirred at room temperature for 1hour (reaction f) to form **9'**. The so formed **5'** and **9'** species were mixed together into a Schlenk flask. Then 0.5% mol of catalyst in dry THF solution (10 mmol/L, 6.35 mL) was added and the mixture was thoroughly stirred for 30 minutes at room temperature. The polymerization was ended by adding few drops of aqueous HCl (5 mol/L). The mixture was poured into petroleum ether (200 mL) and stirred for 45 min. The polymer was collected by centrifugation and washed with water and acetone. The crude polymer was dissolved in chloroform (50°C, 20 mL), and then precipitated again in petroleum ether (300 mL). The product was collected by filtration and then dried in vacuum (800 mbar, 25°C). Yield: 13.55%. $^{1}$H-NMR (128 scan, 50 °C, 600 MHz, $CDCl_3$-d, ppm) δ:6.98 (s, 1H), 2.81 (t, J = 7.9 Hz, 2H), 1.72 (t, J = 7.7 Hz, 2H), 1.40 – 1.26 (m, 6H), 0.92 (t, J = 7.3, 5.5, 2.8 Hz, 3H).

***VI-LM-028:*** The procedure is analogue to the **VI-LM-027's** one. In a Schlenk flask, Grignard derivative **10'** was prepared by mixing **10** (0.0356 g, 0.0522 mmol) with lithium chloride (0.5 M in THF, 0.1 mL, 0.0522 mmol) and *i*PrMgCl (2 M in THF, 0.03 mL, 0.0522 mmol) in dry THF (0.1 mL) under Argon atmosphere. The mixture was stirred at room temperature for 2 hours.Similarly,compound **9** (2.907 g, 7.79 mmol) was mixed with lithium chloride (0.5 M in THF, 15.6 mL, 7.79 mmol), dry THF (38 mL) and *i*PrMgCl (2 M in THF, 3.9 mL, 7.79 mmol)[39]. The mixture was stirred at room temperature for 1 hour (reaction f) to form **9'**. The two obtained Grignard species were mixed together into a Schlenk flask. Then 0.5% mol of catalyst in dry THF solution (10 mmol/L, 0.78 mL) was added and the mixture was thoroughly stirred for 30 minutes at room temperature. The polymerization was ended by adding few drops of aqueous HCl (5 mol/L). The mixture was poured into petroleum ether (75 mL) and stirred for

45 min. The polymer was collected by centrifugation and washed with water and acetone. The crude polymer was dissolved in chloroform (50°C, 20 mL), and then precipitated again in petroleum ether (300 mL). The product was collected by filtration and then dried in vacuum (800 mbar, 25°C). Yield: 8 %. $^1$H-NMR (128 scan, 50 °C, 600 MHz, $CDCl_3$-d, ppm) δ:6.98 (s, 1H), 2.81 (t, J = 7.9 Hz, 2H), 1.72 (t, J = 7.7 Hz, 2H), 1.40 – 1.26 (m, 6H), 0.92 (t, J = 7.3, 5.5, 2.8 Hz, 3H).

***General procedure for Stille-copolymers***. Equimolar amounts of dibromo and bis(tributylstannyl) derivatives were dissolved in dry DMF in a microwave-vial. A catalytic amount of $Pd(PPh_3)_4$ was added and the system was degassed with Argon. The vial was then heated by micro-wave for 5 min at 100°C, 5 min at 120°C and 30 min at 150°C. The polymerization is stopped by the addition of few drops of HCl 5 M. The reaction mixture was poured in methanol and stirred for 1 h. The precipitate is recovered by filtration and purified by Soxhlet extraction (24 h in methanol, 24 h in acetone). The final polymer was dried 24 h at room temperature *in vacuo*.

***GRe-2-12.*** $^1$H-NMR δ (200 MHz, $CDCl_3$-d ppm)= 7.68 (br d, 2 H, 2×CH, benzothiadiazole), 7.27 (s, 2 H, 2×CH, thiophene), 2.70 (br t, 4 H, 2×Ar$CH_2$), 1.66 (m, 4 H, 2×Ar$CH_2CH_2$), 1.26 [m, 12 H, 2 × $CH_3(CH_2)_3$], 0.86–0.83 (br t, 6 H, 2×$CH_3$).

***GRe-2-14***. $^1$H-NMR (600 MHz, $CDCl_3$-d, ppm) δ:7.68 (brd, 2 H, CH, benzothiadiazole), 7.18-7,05 (brs, 4 H, 4×CH, thiophene), 2,55-2,47 (brd, 8 H, 4×Ar$CH_2$), 1.57 (brd, 8 H, 4×Ar$CH_2CH_2$), 1.25 [m, 24 H, 4×$CH_3(CH_2)_3$], 0.88-0.83 (br t, 12 H, 4 × $CH_3$).

***GRe-2-23***. $^1$H-NMR (600 MHz, $CDCl_3$-d, ppm) δ:)= 7.69 (brd, 2 H, CH, benzothiadiazole), 7.18-7.02 (brs, 6 H, 6xCH, thiophene), 2.78-2,58 (brd, 12 H, 6xAr$\underline{CH_2}$) 1.68-1,59 (brd, 12 H, 6xAr$CH_2\underline{CH_2}$), 1.29 [m, 36 H, 6 x $CH_3(\underline{CH_2})_3$], 0.88 (br t, 18 H, 6 x $\underline{CH_3}$).

**2.3 Solar cell fabrication**

Flexible PET/ITO substrates, sized 2.5 x 2.5 $cm^2$, were laser scribed to obtain 4 electrically isolated areas on the same substrate. They were washed with DI water and a mild detergent, rinsed and immersed in IPA to undergo 10 minutes in an ultrasonic bath. After 15 minutes under a UV lamp, an aqueous colloidal dispersion of $SnO_2$ nanoparticles (15% in weight) was spin-coated on the substrates at 6000 rpm for 30 seconds. The deposited $SnO_2$ thin films were annealed in air at 100 °C and treated under UV lamp for 15 minutes prior to perovskite deposition.

For the perovskite precursor solution, 166 mg FAI, 21.6 mg MABr, 87.1 mg $PbBr_2$, 547.4 mg $PbI_2$ and 19.4 mg CsI were dissolved in a mixed solvent of DMF and DMSO at the volume ratio of 3.16:1 and then let to stir for 12 hour at room temperature. The as-prepared precursor solution was then deposited onto PET/ITO/SnO2 via spin coating, first at 1000 rpm for 10 seconds and then at 5000 rpm for 30 seconds. Just 7 seconds before the end of the spinning process, 150 µl of CB was dropped on the substrates. Subsequently, the perovskite layer was annealed at 100°C for 45 minutes.

Spiro-OMeTAD in chlorobenzene (73.5 mg/ml) was employed as the reference hole transporting material (HTM), using 16.6 µl of LiTFSI (520 mg/ml), 7.2 µl of FK209 cobalt(III)TFSI in acetonitrile (0.25 M) and 27 µl of 4-tert-butylpyridine as additives. The solution was spin-coated over the perovskite surface at 2000 rpm for 20 s. All polymer solutions were prepared by dissolving 12 mg of material in 1 ml of chlorobenzene and were doped by adding Li-TFSI, TBP, and Co(III)-TFSI, according to the doping strategy and procedure previously reported[21].To prevent any agglomeration, solutions were kept stirring at 50 °C for 15 min, and eventually deposited by spin-coating at 6000 rpm for 45 seconds.

Finally, the cells were completed by thermal evaporation of Au (80 nm) as the top electrode. The devices were masked with an aperture of 0.09 $cm^2$ to define the active working area.

**2.4 Module fabrication**

PET/ITO was etched with a UV Nd:YVO4 laser beam to obtain the layout of the modules (P1 ablation). The module layout consists of 8 series-connected cells with 4.5 mm as cell width and with an overall active area of 16 $cm^2$. The module aperture ratio, i.e. the ratio between the active area and the aperture area, is approximately 87%. After the P1 laser ablation, the patterned substrates were cleaned in an ultrasonic bath, using detergent with de-ionized water and isopropanol (10 minutes for each step). The same materials and solutions as for the small cells were used for the modules. $SnO_2$, perovskite and HTM were spin coated onto the laser patterned ITO plastic substrates (6x6 $cm^2$). The spin-coating parameters for perovskite, Spiro-OMeTAD and VI-LM-027 were optimized for the larger area. The P2 laser ablation was performed to selectively remove materials from the interconnection areas. The laser parameters optimized to remove the $SnO_2$/Perovskite/HTM stack were: laser pulse power of 43 mW, Raster Scanning Distance (RSD) of 70 µm, 100 mm/s ablation rate. Au back contacts (nominal thickness 100 nm) were thermally evaporated in a high vacuum chamber ($10^{-6}$ mbar). Finally, P3 laser ablation was performed to obtain the electrical insulation between the counter-electrodes of adjacent cells, using the following parameters: 74 mW of power pulse, RSD of 18 µm and 195 mm/s ablation rate.

**2.5 Characterisation**

$^1$H-NMR spectra (200 MHz or 600 MHz) were recorded using respectively a Bruker Avance 200 Spectrometer or JEOL ECZ-R 600, with TMS as internal standard in deuterated solvents.

Chemical shifts are reported in ppm and coupling constant (J) in Hz. Flash chromatography was performed on Biotage Isolera One instrument. TLC were carried out on silica gel 60 F254 plates. All microwave polymerizations were performed on Biotage Initiator 2.5. UV-Vis analyses were recorded with a Shimadzu PharmaSpec 1700 spectrometer, while fluorescence spectra with a Horiba Jobin Yvon Fluorolog. Cyclovoltammetry measurements were performed on a BioLogic sp150 using tetrabutylammonium hexafluorophosphate in chloroform (0.1 M) with a scan speed of 50 mV/s. Thermal stability was evaluated by thermogravimetric analyses under nitrogen, using a SDT Q600 V20.9 Build 20 instrument.

The gel permeation chromatographic analysis was carried out with a Viscotek 270 instrument, a Tetra Detector system and a set of two columns T6000M Viscotek (300 x 8 mm); chloroform was used as a carrier solvent (flow rate: 1 mL/min, 30°C) and the calibration was performed with narrow polystyrene standards. Sample solutions (0.4-0.5% w/v) were prepared at room temperature and then filtered on 0.45 μm PTFE filters.

Current density-voltage (J-V) curves were recorded using a class AAA solar simulator (Newport) and an automated measuring system (Arkeo-Ariadne, Cicci Research s.r.l.). The illumination was set to AM1.5 and calibrated to 100 mW/cm$^2$ using a calibrated silicon reference cell. The cells were measured in both forward and reverse direction with a scan rate of 100 mV/s. The active area was controlled by using a dark mask with an aperture of 0.09 cm$^2$. For the stability measurement, the unencapsulated devices were tested under white LEDs at 1 equivalent sun in ambient conditions. The MPP was measured via perturb and observe algorithm implemented onto a commercial apparatus (Arkeo-Ariadne, Cicci Research s.r.l.) based on a set of 4-wire independent source meters.

EQE spectra were recorded using a commercial setup (Arkeo-Ariadne, Cicci Research srl) based on a 300 W xenon lamp, able to acquire a spectrum from 300 to 1100 nm with a resolution of 2 nm.

## 3. Results and discussion

### 3.1 Tailoring polymer properties by thoughtful choice of the synthetic procedure

The first synthetic approach relied on the preparation of appropriate stannyl derivatives, followed by a Stille-based copolymerization (Scheme 1a and b), to produce three different copolymers, following a reported procedure [29]. A benzothiadiazole **1** was first dibrominated by NBS to **2** and then used in a Suzuky-Miyaura cross coupling with commercially available thiophene **3** to provide the BDT-based monomer **4.** A lithiation at low temperature on **4** followed by quenching with tributyl tin chloride provided the reactive monomer **6**. The final polymerization was carried out under microwave irradiation leading three different polymers, spacing two adjacent BTDs by two, four and six HT units (**GRe-2-12**, **GRe-2-14**, **GRe-2-23** respectively). Upon a final purification by Soxhlet extraction the final polymers where characterized by a higher molecular weight and better yields in comparison to the analogues obtained by classical thermal heating reactions [29]. The Stille approach is characterized by a remarkable versatility and feasibility, nevertheless toxicity and harmfulness of the organic tin derivatives undermine its sustainability [35,36]. To overcome these limitations, Kumada polycondensation was explored as greener alternative to obtain polymers characterized by higher molecular weight and regioregularity [37]. In the latter, the BDT concentration in the P3HT backbone could be tuned to very low values avoiding the tedious synthesis of specific oligomers. Two functionalized monomers **5** and **9** were treated with Grignard reagent to

prepare *in situ* the reactive monomers **5'** and **9'**by metathesis reaction. The latter was specifically employed instead of the dibromo analogue to selectively promote the generation of the Grignard species replacing the iodine on the thiophene scaffold. Finally, the reactive Grignard monomers were mixed in dry THF with freshly prepared Ni(IPr)$(acac)_2$ (Scheme 1C), to prepare polymers **VI-LM-027** and **VI-LM-028** [38]. It is worth nothing that the nickel catalyst was chosen due to well-established features to control the polydispersity and to promote the formation of high molecular weight polymers which are both desirable features for applications in cells. As widely known, the molecular weight of the final polymers can be modulated operating on the molar percentage of the catalyst in the reactive mixture [39]. Benzothiadiazole was selected as electronic-deficient moiety in the synthesis of donor-acceptor polymers since it has shown remarkable properties both in photovoltaics and organic electronics fields [40–42]. Relatively low HOMO energy level allows a good resistance against oxidative damage and thus better device performance.

In parallel, a diketopyrrolopyrrole (DPP, **VI-LM-028**) moiety was also inserted by Kumada polycondensation instead of BTD to improve the solubility and the charge mobility (Scheme 1C). The $\pi$-interaction between the DPP carbonyl groups and the thiophene sulphur leads to a better solid-state packing and to a high crystallinity degree [43].

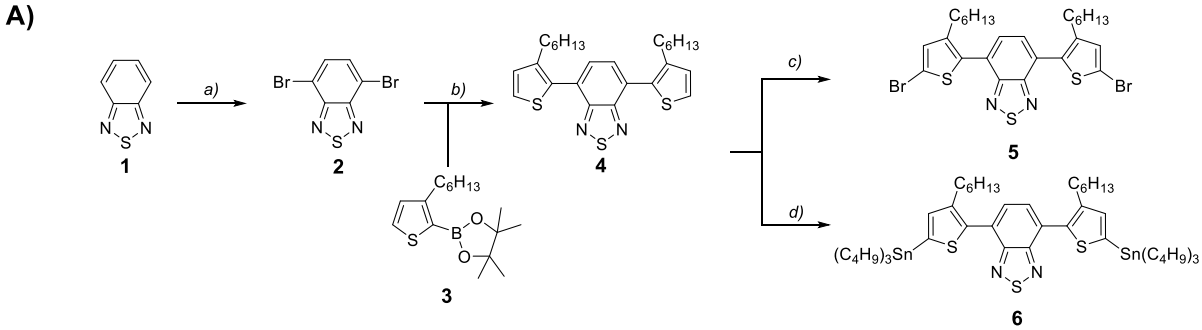


*a)* NBS, $H_2SO_4$, 60°C, 3h; *b)* **3**, $K_2CO_{3(aq.)}$, $Pd(PPh_3)_4$, toluene, 100°C, 12 h; *c)* NBS, THF, 0°C to rt, overnight; *d)* BuLi, $SnBu_3Cl$ THF, -80°C to rt, 12 h.

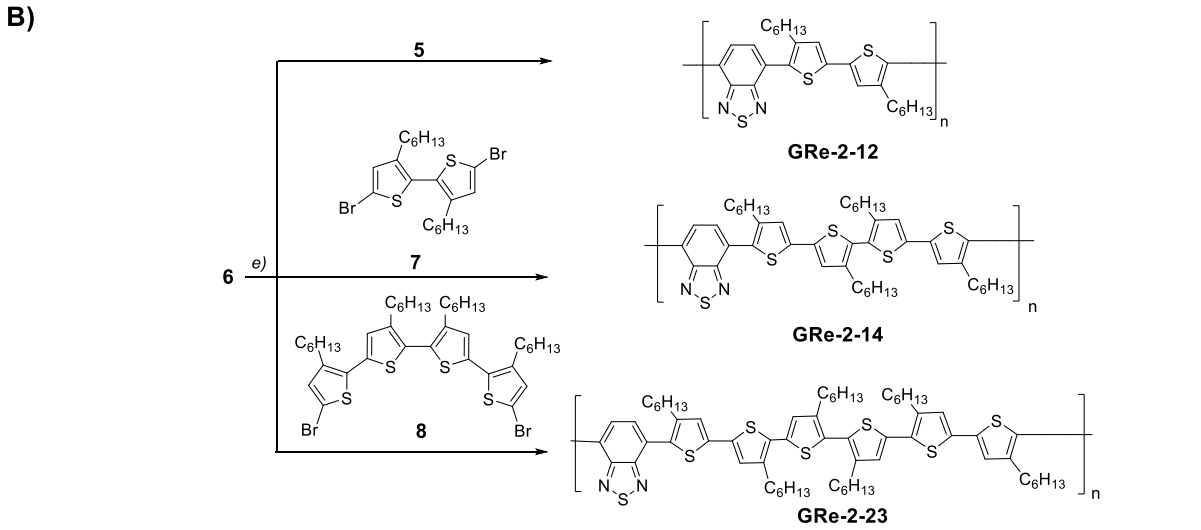


*e)* dibromo compound, $Pd(PPh_3)_4$, DMF, MW irradiation, 5' at 100°C, 5' at 120 °C, 30' at 150°C.

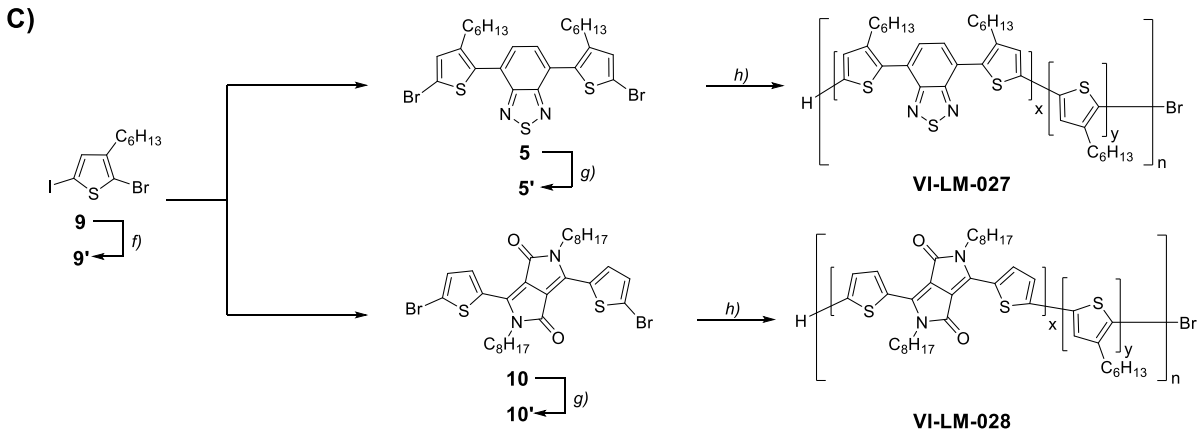


*f)* iPrMgCl, LiCl, THF, rt, 1 h; *g)* iPrMgCl, LiCl, THF, rt, 2 h; *h)* $Ni(iPr)(acac)_2$, rt, 0.5 h

Scheme 1. *Synthetic strategy of different polymers: synthesis of precursors (A); Stille reaction (B); Kumada reaction (C).*

### 3.2 Characterization of the materials (NMR, Thermal, MW, opto-electronic)

As already discussed in the synthetic section, Kumada approach does not allow a fine control of the stoichiometry of the obtained polymer. Thus, the HT/BDT ratio could not be known *a*

*priori.* In this context, to investigate the exact structure of co-polymer **VI-LM-027**, we resolved to elemental analyses. Unfortunately, we were not successful in structure elucidation. No nitrogen signal was detected whereas the sulphur amount could be ascribable to both a pure P3HT or a BDT/P3HT copolymer (with an amount of BDT/3HT ratio lower than 1:16). For further discussion on this topic please see

and the related discussion. Albeit an unambiguous evidence of the presence of BDT in **VI-LM-027** polymer was not found by both elemental analyses and NMR, the differences between the VI-LM_027 and P3HT can be evidenced by the indirect measures reported in Table 1 where, , both opto-electronic and thermal properties of **VI-LM-027** differ from the ones of a pure P3HT. Considering the trend of the latter a fair estimation of the BDT/3HT ratio in **VI-LM-027** is 1:35, that justifies the undetectability of the Nitrogen signal in the elemental analyses.

| | ***MW [kg*mol$^{-1}$][a]*** | ***PDI[a]*** | ***$\lambda_{abs}$ [nm]*** | ***$E_{HOMO}$ [eV] [b]*** | ***$T_d$ [°C] [c]*** | ***$\delta$(CH $_{thioph}$) [ppm][d]*** |
|---|---|---|---|---|---|---|
| ***GRe-2-12*** | *4.84* | *1.46* | *321, 474* | *-5.52* | *432* | *7.27* |
| ***GRe-2-14*** | *-* | *-* | *379* | *-5.44* | *451* | *7.11* |
| ***GRe-2-23*** | *7.32* | *1.19* | *400* | *-5.30* | *461* | *7.02* |
| ***VI-LM-027*** | *44.9* | *1.25* | *453* | *-5.14* | *479* | *6.98* |
| ***P3HT-94*** | *94* | *-* | *469* | *-5.00/-5.10* | *485* | *6.98* |

Table 1. Characterization of BTD-based synthesized polymers and commercial P3HT (94 kDa)


| | ***MW [kg*mol$^{-1}$][a]*** | ***PDI[a]*** | ***$\lambda_{abs}$ [nm]*** | ***$E_{HOMO}$ [eV] [b]*** | ***$T_d$ [°C] [c]*** | ***$\delta$(CH $_{thioph}$) [ppm][d]*** |
|---|---|---|---|---|---|---|
| ***GRe-2-12*** | *4.84* | *1.46* | *321, 474* | *-5.52* | *432* | *7.27* |
| ***GRe-2-14*** | *-* | *-* | *379* | *-5.44* | *451* | *7.11* |
| ***GRe-2-23*** | *7.32* | *1.19* | *400* | *-5.30* | *461* | *7.02* |
| ***VI-LM-027*** | *44.9* | *1.25* | *453* | *-5.14* | *479* | *6.98* |
| ***P3HT-94*** | *94* | *-* | *469* | *-5.00/-5.10* | *485* | *6.98* |


*[a]: Calculated by GPC (eluent $CHCl_3$, 30 °C, 1 mL/min, narrow polystyrene standards). [b] Calculated by CV analysis ($CHCl_3$, TBA as supporting electrolyte, 25 °C, 50 mV/sec). [c] Calculated by TGA analysis under $N_2$ atmosphere (heating ramp 10°C/min). [d] Chemical shift measured with a 600 MHz NMR (in deuterated $CHCl_3$).*

### 3.3 NMR structural information

$^{1}$H-NMR analysis was used to confirm the structures of the obtained copolymers. The peaks' shape in the NMR spectra of Stille-derived copolymers and their good solubility at room temperature suggest lower molecular weights than Kumada's one. **VI-LM-027** requires, indeed, higher temperatures ($\sim$ 50°C) to reach a completely dissolution into chloroform for the analysis. The BTD/HT ratio along the polymeric backbone dramatically influenced the resonance frequency of the thiophenic proton in the 4-position on the ring. The higher the ratio, the higher the chemical shift of the aromatic proton due to the electronic effects of the acceptor unit (Figure 1). A trend can be observed starting from **GRe-2-12** where this proton resonates at 7.27 ppm until to **VI-LM-027**, where the same atom shows its own peak at 6.98 ppm, going through **GRe-2-14** (7.08 ppm) and **GRe-2-23** (7.02 ppm). The $\alpha$-methilene group is strongly affected by the chemical environment and regioregularity of the system too. It resonates at different frequency depending on its proximity to an Head-to-Tail coupling rather than Tail-to-Tail or Head-to-Head ones [44]. In particular, a unique large broad peak can be observed at 2.5 ppm for **GRe-2-12**, whereas **GRe-2-14** and **GRe-2-23** have several peaks between 2.5 and 2.7 ppm due to a more regio-random orientation of the alkyl chains. **VI-LM-027** is the most regioregular system: a unique narrow peak can be attributed to the $\alpha$-methilene group. According to a common procedure reported in literature [45], RR has been estimated of almost 100%.

It should be pointed out that the RR has its own meaning only if homopolymer is considered. In case of co-polymer (as the present case is), the RR accounts mainly for the ordering of the different monomeric units. According to the NMR-analysis, no traces of BTD moiety are detectable in the **VI-LM-027** polymer due to the low sensitivity of the technique (> 5%) and the extremely low BTD/HT ratio characterizing this polymer. Further analyses were carried out and reported below in order to discriminate it from a bare P3HT.

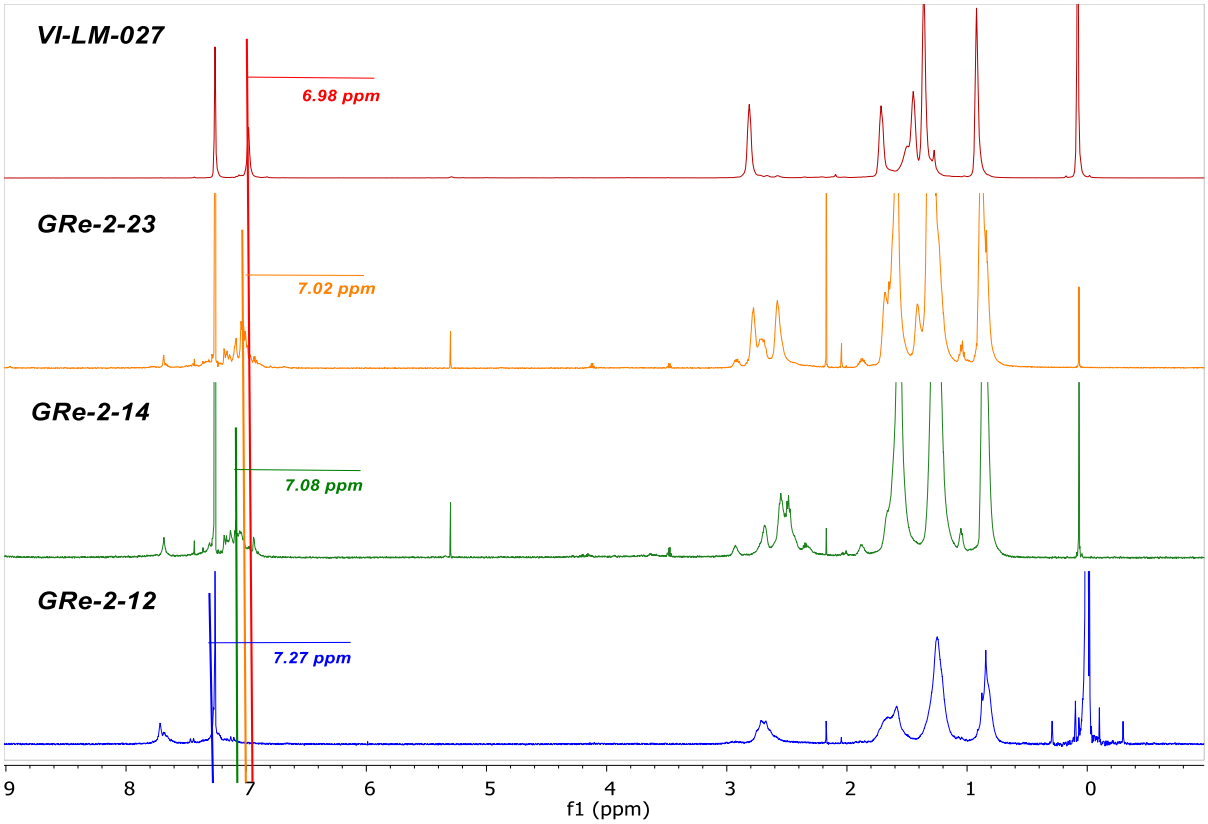


Figure 1. NMR spectrum of VI-LM-027 (red), GRe-2-23 (orange), GRe-2-14 (green) and GRe-2-12 (blue). Vertical lines evidenced the shift of the proton in the thiophene ring following on from the modification of the chemical environment, i.e. the presence and the proximity of the benzothiadiazole moiety. The same proton in a fully RR homopolymer P3HT resonates at 6.98 ppm (in deuterated $CHCl_3$).[24]

### 3.4 Thermal stability

Thermal stability of the polymers was evaluated by Thermogravimetric Analyses (TGA). The decomposition temperature ($T_d$) reported in

has been evaluated as the maximum of the derivative of the related TGA curve. Kumada

| | ***MW [kg*mol$^{-1}$][a]*** | ***PDI[a]*** | ***$\lambda_{abs}$ [nm]*** | ***$E_{HOMO}$ [eV] [b]*** | ***$T_d$ [°C] [c]*** | ***$\delta$ (CH $_{thioph}$) [ppm][d]*** |
|---|---|---|---|---|---|---|
| ***GRe-2-12*** | *4.84* | *1.46* | *321, 474* | *-5.52* | *432* | *7.27* |
| ***GRe-2-14*** | *-* | *-* | *379* | *-5.44* | *451* | *7.11* |
| ***GRe-2-23*** | *7.32* | *1.19* | *400* | *-5.30* | *461* | *7.02* |
| ***VI-LM-027*** | *44.9* | *1.25* | *453* | *-5.14* | *479* | *6.98* |
| ***P3HT-94*** | *94* | *-* | *469* | *-5.00/-5.10* | *485* | *6.98* |

copolymer shows the highest $T_d$. The insertion of BTD moiety may lead to an easier fragmentation of the polymeric chains, lowering the decomposition temperature. This well correlates with the observed $T_d$ decrease (**GRe-2-12** < **GRe-2-14** < **GRe-2-23** < **VI-LM-027** <

**commercial P3HT**). In Figure S1A, it can be noticed that **VI-LM-027** curve exhibits a 10% loss around 100°C that persists also after a treatment of the sample under vacuum overnight at 40°C. This may be rationalized with a high hygroscopicity of the system, not observed for the Stille products.

### 3.5 Molecular Weights

The molecular weights and their distribution (PDI) have been evaluated by gel-permeation chromatography (GPC), using chloroform as eluent carrier (T = 30 °C, flowrate 1 mL/min) and narrow polystyrene standards for calibration. Stille copolymers were soluble in the most common organic solvent at room temperature, while **VI-LM-027** was harder to dissolve. GPC chromatogram show that **VI-LM-027** has the highest molecular weight ($M_n$ = 45 kg/mol, PDI = 1.25), followed by **GRe-2-23** and **GRe-2-12** (Figure S1B). **GRe-2-14**'s MW has not been evaluated since it was just synthesized as an intermediate step going from **GRe-2-12** to **GRe-2-23**, useful for electrochemical and optical properties monitoring, but lacking an application as HTM in the solar cell. Looking at Figure S1B, it's clear that Stille copolymers exhibit lower molecular weights than **VI-LM-027** ($M_n$< 10 kg/mol, PDI < 1.5). In particular, **GRe-2-12**'s MW is lower than **GRe-2-23** one, confirming the observation of El-Shehawy *et al.*who supposed that, keeping constant the polymerization method, increasing 3HT moieties along the polymeric backbone improves solubility as well as molecular weights [29].

### 3.6 Optoelectronic characterization

The investigation of frontier molecular orbitals is of paramount importance to assess the suitability of a polymer to be applied as HTM in PSCs. Indeed, the HOMO of the polymer should be positively shifted with respect to the conduction band of the perovskite layer to

assure an effective hole transfer from the PSK to the HTM (actually, an electron will be injected from HTM to PSK). Cyclic voltammetry (CV) is the technique of election to detect the energy level of the HOMO (associated to an oxidation reaction) of both small molecules and polymers. In some cases, also the energy level of the LUMO (associated to a reduction reaction) could be evidenced. If LUMO is not directly accessible from CV, it could be easily calculated from the difference between HOMO energy and the band gap (BG), the energetic distance between HOMO and LUMO, about which UV-Vis absorption and emission analyses could give meaningful information.

As already highlighted by El-Shehawy et al., the frontier molecular orbitals are sensibly influenced by the BTD/HT ratio. The energy of the LUMO level is directly correlated to the amount of BDT being the acceptor unit the preferential delocalization site for the photogenerated hole. We also find an interesting correlation between the energy of the HOMO level and the BTD/HT ratio (

). The higher the BDT/HT ratio the more downshifted the HOMO level: it is shifted from -5.52 eV for **GRe-2-12** (1:2) to -5.44 eV for **GRe-2-14** (1:4) to -5.30 eV for **GRe-2-23** (1:6). Concerning **VI-LM-027**, HOMO is further upshifted up to -5.14 eV that is still lower than commercial P3HT (i.e. -5.00 eV). This trend in the HOMO level further confirms the nature of VI-LM-027 being a halfway point between pure P3HT and Stille-synthetized copolymers (Figure 2A).

| | ***MW [kg*mol$^{-1}$][a]*** | ***PDI[a]*** | ***$\lambda_{abs}$ [nm]*** | ***$E_{HOMO}$ [eV] [b]*** | ***$T_d$ [°C] [c]*** | ***$\delta$ (CH $_{thioph}$) [ppm][d]*** |
|---|---|---|---|---|---|---|
| ***GRe-2-12*** | *4.84* | *1.46* | *321, 474* | *-5.52* | *432* | *7.27* |
| ***GRe-2-14*** | *-* | *-* | *379* | *-5.44* | *451* | *7.11* |
| ***GRe-2-23*** | *7.32* | *1.19* | *400* | *-5.30* | *461* | *7.02* |
| ***VI-LM-027*** | *44.9* | *1.25* | *453* | *-5.14* | *479* | *6.98* |
| ***P3HT-94*** | *94* | *-* | *469* | *-5.00/-5.10* | *485* | *6.98* |

UV-Visible analysis (Figure 2B) was then conducted to evaluate light absorption properties (*e.g.* absorption maximum, band gap). **VI-LM-027** absorption maximum shifts to lower energy

if compared to Stille-copolymers due to a more extended conjugation. This may be rationalized by its greater regioregularity that leads to a more planar system and, consequently, to a greater effective conjugation length [24]. The molecular weight is another key parameter able to affect the absorption features: lower values lead to ipsochromic shift due to a shorter conjugation [46]. These considerations seem to well rationalize the observed difference of at least 50 nm between the two copolymers series.

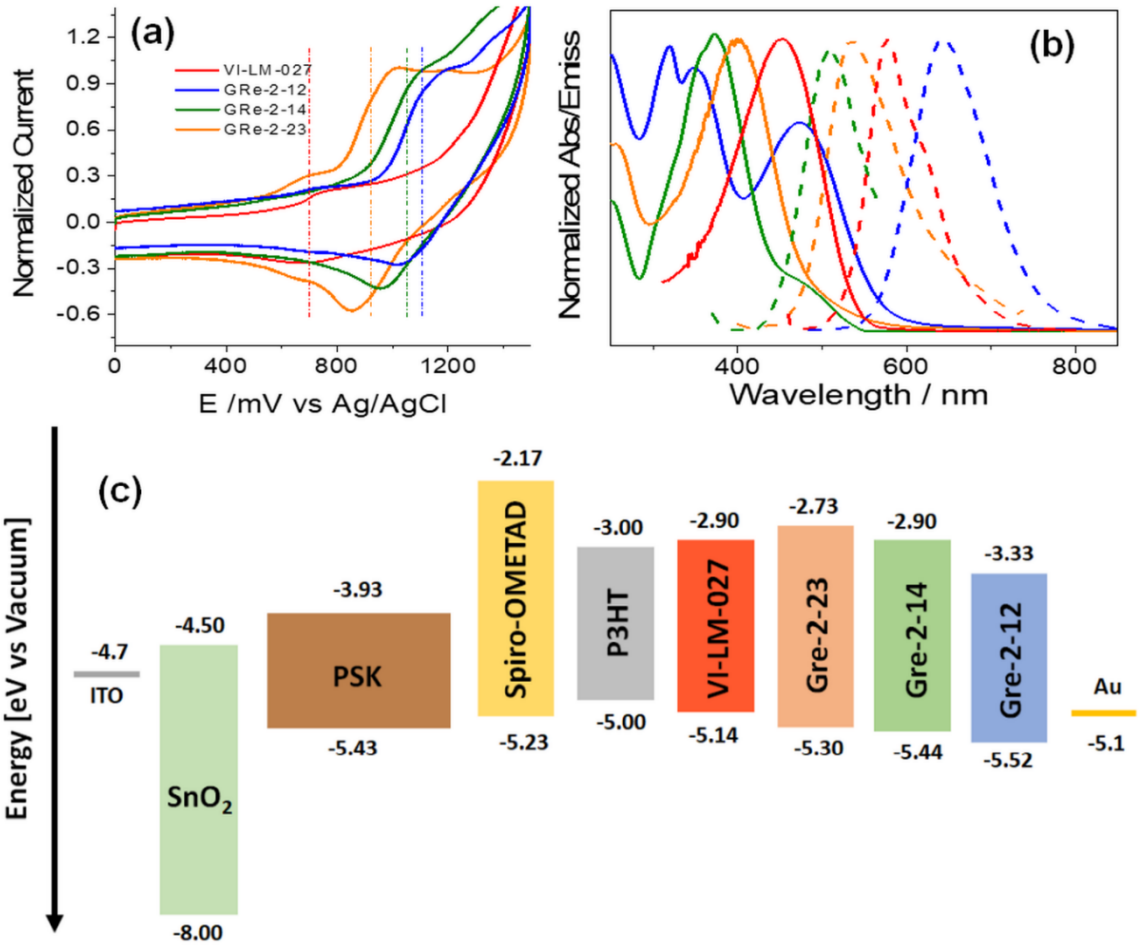


Figure 2. (a) Cyclic voltammetry and (b) optical characterization: absorbance (solid) and emission (dashed). Spectra are normalized and recorded in $CHCl_3$. (c) Sketch of the energy levels of the materials employed throughout this work.

### 3.7 Flexible perovskite solar cells

The synthesised polymers were employed as hole transport materials (HTM) in perovskite solar cells on flexible substrates with n-i-p structure: PET/ ITO/ $SnO_2$/

$Cs_{0.06}FA_{0.78}MA_{0.16}Pb(I_{0.84}Br_{0.16})_3$/ HTM/ Au. Commercially available P3HT with different molecular weights (i.e. 21, 54 or 94 kDa) and spiro-OMeTAD were employed as reference materials.

As reported in Figure 3, the reference cells with spiro-OMeTAD delivered in average 13% power conversion efficiency (PCE), with short circuit current density ($J_{SC}$) ranging between 17.4 and 19.7 mA/cm$^2$, open circuit voltages ($V_{OC}$) of 1049 to 1080 mV and fill factors (FF) of 65% in average. Among the commercially available P3HTs, whose increasing trend of the PV parameters with the molecular weight is reported in **Errore. L'origine riferimento non è stata trovata.**, the best performing cells were obtained with P3HT-94kDa, as expected from previous reports[33], attaining 10.1% PCE in average and a maximum of 11.3% (reverse scan). Interestingly, **VI-LM-027** showed comparable efficiency to P3HT-94, i.e. average 9.2% and best 10.8% PCE (reverse scan), confirming the low incorporation degree of BDT in the P3HT backbone. The two polymers delivered very similar $J_{SC}$ in average (P3HT-94: 16.4 mA/cm$^2$ in reverse, 16.6 mA/cm$^2$ in forward direction; **VI-LM-027:** 16.6 mA/cm$^2$ in reverse, 16.4 mA/cm$^2$ in forward direction), with the highest values reached by the commercial P3HT, although with a larger spread. $V_{OC}$ values were also more scattered for P3HT-94, ranging between 921 mV and 1039 mV, and higher in average than **VI-LM-027** (992 mV and 947 mV in reverse direction, respectively); average FF did not differ much either, being 61% in reverse and 54% in forward for P3HT-94, 58% in reverse and 55% in forward for **VI-LM-027.**

Stille-synthesized HTMs afforded worse PCEs, below 6%, as one would expect due to their lower molecular weight: **GRe-2-12** and **GRe-2-23** yield comparable $V_{OC}$ of around 815 and 790 mV respectively, but very different $J_{SC}$ up to 14 mA/cm$^2$ in average, with peaks of 15.8 mA/cm$^2$

for **GRe-2-12,** whereas very scattered values were recorded for **GRe-2-23,** all below 10 mA/cm$^2$.

The lower $V_{OC}$ delivered by all polymers, although to different degrees, can be ascribed to additional non-radiative recombination at the perovskite/polymer interface and lower electron lifetime compared to spiro-OMeTAD, possibly caused by a strong electronic coupling between flat P3HT and perovskite and also by physically poor contact, impeding efficient hole transport from the perovskite to the polymer [6]. The striking $V_{OC}$ gap, i.e. almost 200 mV, between the Stille-synthesized polymers and **VI-LM-027** is most likely due to the noticeable difference in MW, below 30 kDa and over 65 kDa respectively, that has been demonstrated to be related to charge recombination [33]. The faster recombination associated with low MW explains the lower $J_{SC}$ and FF of the solar cells based on **GRe-2-12** and **GRe-2-23.** The difference in $V_{OC}$ between **VI-LM-027** and commercial P3HT-94 instead is not so remarkable,

even though the MW of the latter is around 30 kDa higher than the former, that is the same divide between **VI-LM-027** and the GRe-2 polymers.

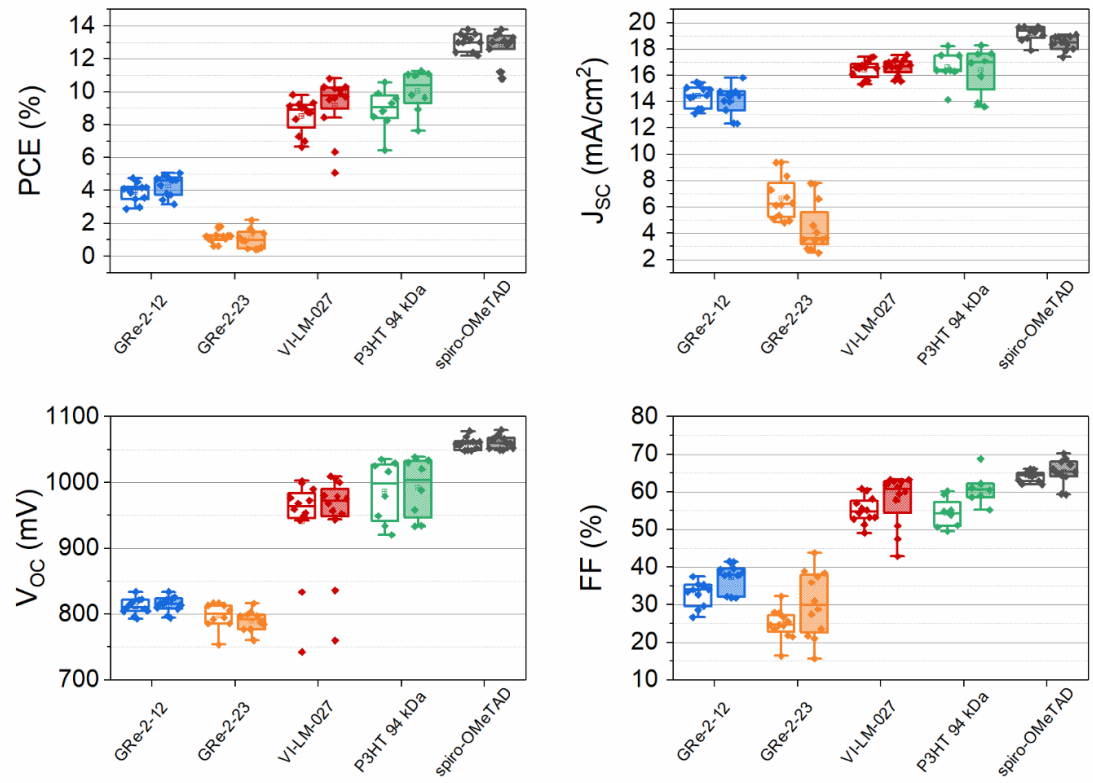


Figure 3. PV parameters of the flexible PSCs endowed with the different HTMs synthesised for this study. Cells with commercially available P3HT (MW = 94 kDa) and spiro-OMeTAD were fabricated and used as reference.

The J-V curves of the best devices, whose PV parameters are reported in Table 2, in both forward and reverse directions are shown in Figure 4A. The curve shape for **GRe-2-12** and **GRe-2-23** reveals issues with the conductivity through the layers, possibly due to far from optimal PSK/HTM and/or HTM/Au interfaces. Indeed, relatively high BDT concentration could negatively influence the planarity of the system and, therefore, the charge transport throughout the HTM, as also confirmed by the low value of FF for both **GRe-2-12** and **GRe-2-23** [47]. It should be pointed out that, for all the investigated HTMs, the hysteresis is very small. External quantum efficiency (EQE) spectra of the same cells are reported in Figure 4B

alongside the corresponding integrated photocurrents, whose values are in good agreement (± 5%) with the $J_{SC}$ values measured under solar simulator; the only exception is **GRe-2-23** that showed a 50% increase with respect to the $J_{SC}$ measured by the J-V scan, possibly due to higher recombination rates and/or less effective charge transport under full illumination.

Based on the interesting results obtained with **VI-LM-027** and its superior photoelectrochemical properties with respect to Stille-synthesized HTMs, we developed a new polymer (**VI-LM-028**), bearing a different acceptor unit, namely a diketopyrrolopyrrole (DPP) moiety. Once implemented in PSCs, though, it showed very poor PCE, below 1% (see **Errore. L'origine riferimento non è stata trovata.**) and it was not further investigated. The very low efficiency value is probably ascribable to both a not optimal energy level of frontier orbitals (HOMO = -5.39 eV and LUMO = -3.14 eV) and a more hindered structure of DPP compared to BDT that negatively influences the planarity of the resulting polymers [47].

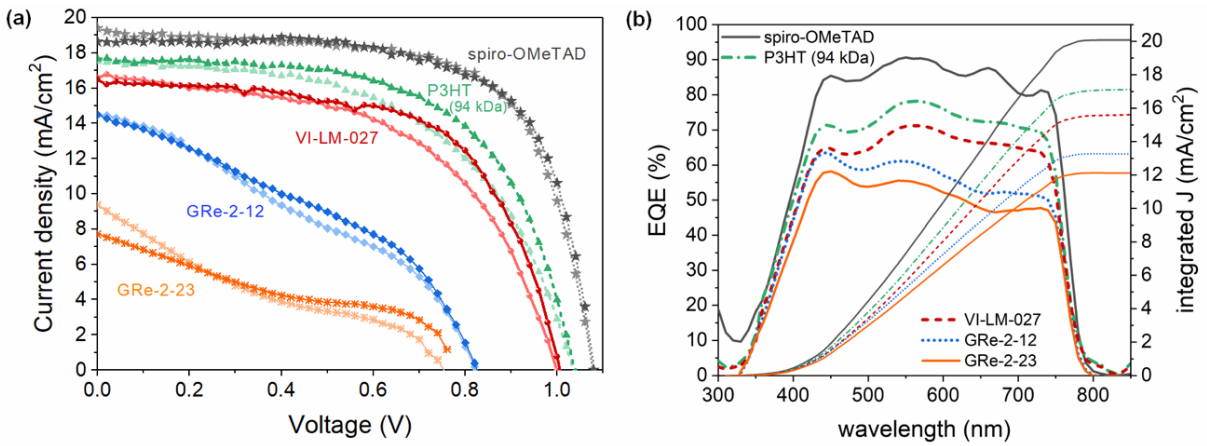


Figure 4. Best flexible PSCs with different HTM materials: (a) J-V curves in both reverse (darker symbols) and forward (lighter symbols) scan directions; (b) EQE spectra and photocurrent values calculated from their integration.

Table 2. PV parameters for the best flexible PSCs endowed with different HTMs.

| HTM | | $V_{OC}$ (V) | $J_{SC}$ (mA/cm$^2$) | FF (%) | PCE (%) |
|---|---|---|---|---|---|
| **GRe-2-12** | *FWD* | *0.834* | *15.4* | *35.4* | *4.54* |
| | REV | 0.834 | 14.5 | 39.6 | 4.79 |
| **GRe-2-23** | *FWD* | *0.754* | *9.38* | *24.5* | *1.73* |
| | REV | 0.760 | 7.72 | 37.5 | 2.20 |
| **VI-LM-027** | *FWD* | *1.003* | *16.7* | *55.1* | *9.24* |
| | REV | 1.009 | 17.1 | 62.7 | 10.8 |

| | | | | | |
|---|---|---|---|---|---|
| **P3HT (94 kDa)** | *FWD* | *1.035* | *17.5* | *54.8* | *9.92* |
| | REV | 1.039 | 17.6 | 60.6 | 11.1 |
| **Spiro-OMeTAD** | *FWD* | *1.078* | *19.4* | *66.1* | *13.8* |
| | REV | 1.080 | 18.6 | 68.8 | 13.8 |

Furthermore, we tested the operational stability of unencapsulated devices with the most promising in-house synthetized polymer, i.e. **VI-LM-027**, under continuous 1-equivalent sun illumination from white LEDs, in air at room temperature and ambient humidity (about55% RH), by tracking their maximum power point. Devices with spiro-OMeTAD and P3HT-94 were also tested at the same time as a reference. The efficiency of all cells, regardless the HTM, dropped remarkably after just half an hour, as reported in Figure 5A: in average, **VI-LM-027**, P3HT-94 and spiro-OMeTAD lost around 20%, 30% and 50% of their initial performance respectively. Afterwards, while spiro-OMeTAD efficiency kept degrading exponentially, losing 90% of its initial efficiency after just 2 hours, **VI-LM-027** experienced a less severe degradation rate, reaching 60% and 30% after 6 and 15 hours of exposure, respectively; once more, P3HT-94 showed an intermediate stability, yet evidently lower than BDT-modified P3HT. The efficiency trend replicates closely the $J_{SC}$ evolution with time (Figure 5B); $V_{OC}$ remained stable for the polymers, but it dropped significantly for spiro-OMeTAD, showing a large dispersion due to a larger failure of one of the two devices tested (**Errore. L'origine riferimento non è stata trovata.**a); spiro-OMeTAD as well as P3HT-94 experienced an initial FF decrease of 40% and 20% respectively reaching a very similar 30% drop by the end (**Errore. L'origine riferimento non è stata trovata.**b). The stability test was stopped after 16 hours and the EQE spectra for **VI-LM-027** and spiro-OMeTAD were recorded and compared to the spectra measured before the light soaking test (**Errore. L'origine riferimento non è stata trovata.**). Spiro-OMeTAD cells suffered an EQE drop of over 90% whereas EQE of **VI-LM-027** devices experienced a 50% reduction in the same testing interval, confirming the $J_{SC}$ evolution with time. Although the

stability test was run at ambient conditions, continuously illuminated devices experienced temperatures around 45 °C, which could explain the faster degradation of cells with spiro-OMeTAD compared to those with VI-LM-027, whose decomposition temperature is higher than 400 °C, as found by TGA.

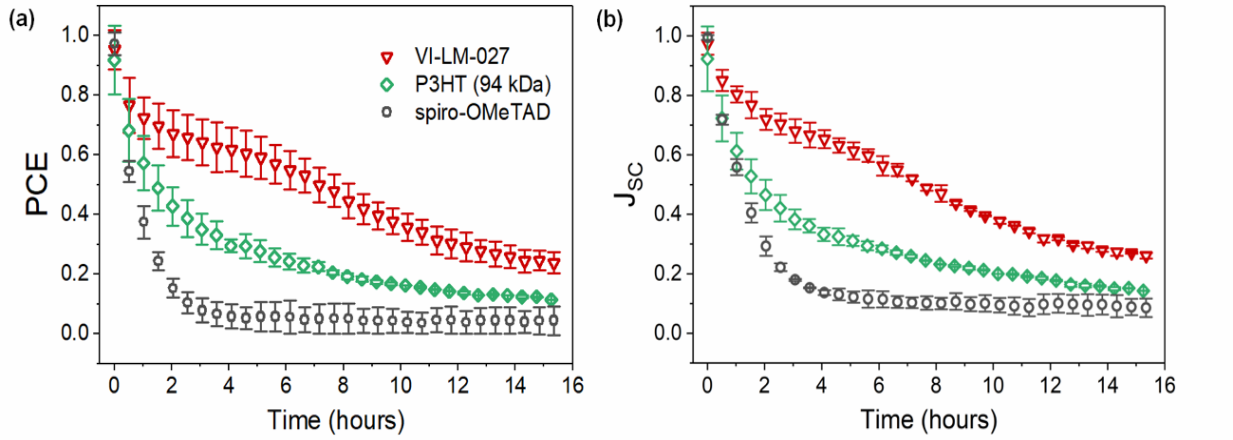


Figure 5. Light soaking test: (a) power conversion efficiency and (b) short circuit current density evolution with time of unencapsulated flexible PSCs. PV parameters were extracted by J-V curve scans run every 30 minutes; in between, devices were kept under load by tracking their maximum power point. Two cells per type were measured and the average values plotted. Though T80 is reached in less than 1 hour for both HTMs, VI-LM-027 display a slower degradation rate than spiro-OMeTAD.

Finally, we demonstrated the potential of the **VI-LM-027** polymer as a low-cost alternative to spiro-OMeTAD, in the crucial and much needed technological transfer from lab scale to industrial manufacture, by spin coating it on a large 6 x 6 $cm^2$ substrate to fabricate working flexible modules. The 8 series-connected cells forming the module were obtained via laser ablation of P1, P2 and P3 [48], resulting in a non-active area for the interconnection between adjacent cells of around 600 μm and, thus, to an aperture ratio of approximately 87% (Figure 6A). Spiro-OMeTAD was used as reference for the necessity of having a ubiquitous standard for easy comparison with literature data. When moving from small to large area, some performance losses in the modules are expected with respect to the lab cell performance. In this case, the spiro-OMeTAD module experienced higher losses than VI-LM-027 as resulting

by comparing the module PV parameters, extracted from the J-V curves (Figure 6C) and reported in **Errore. L'origine riferimento non è stata trovata.**, to those of the best small cells (Table 2).The module $J_{SC}$ resulted to be 5 to 11% lower than the small cell case for VI-LM-027 and 5 to 9% lower for spiro-OMeTAD. The module $V_{OC}$, expected to be ~ 8 V for VI-LM-027 and ~8.6 V for spiro-OMeTAD ($V_{OC}$ of the single cell multiplied by the number of cells), was 4 to 13% and 22 to 25% lower, respectively. The module FF was 26 to 31% lower than the small cell value for **VI-LM-027** and 40 to 46% lower for spiro-OMeTAD. These mismatches, especially in $V_{OC}$ and FF, demonstrate further improvements are still needed, especially in the optimisation of the laser processing, to ensure more effective interconnections via a complete yet selective removal of the layers to minimize recombination and enhance charge transfer. Still, both modules worked with comparable efficiency, delivering over 6% PCE on 16 $cm^2$ of active area. The **VI-LM-027** module in particular reached 6.88% PCE, proving to be a promising HTM candidate in the run towards the realization of commercial perovskite solar cells.

Table 3. PV parameters for the flexible modules.

| HTM | | $V_{OC}$ (V) | $J_{SC}$ (mA/cm$^2$) | FF (%) | PCE (%) |
|---|---|---|---|---|---|
| **Spiro-OMeTAD** | *FWD* | *6.44* | *17.7* | *36.6* | *5.22* |
| | REV | 6.73 | 17.7 | 41.1 | 6.12 |
| **VI-LM-027** | *FWD* | *6.94* | *15.8* | *37.7* | *5.18* |
| | REV | 7.74 | 15.2 | 46.7 | 6.88 |

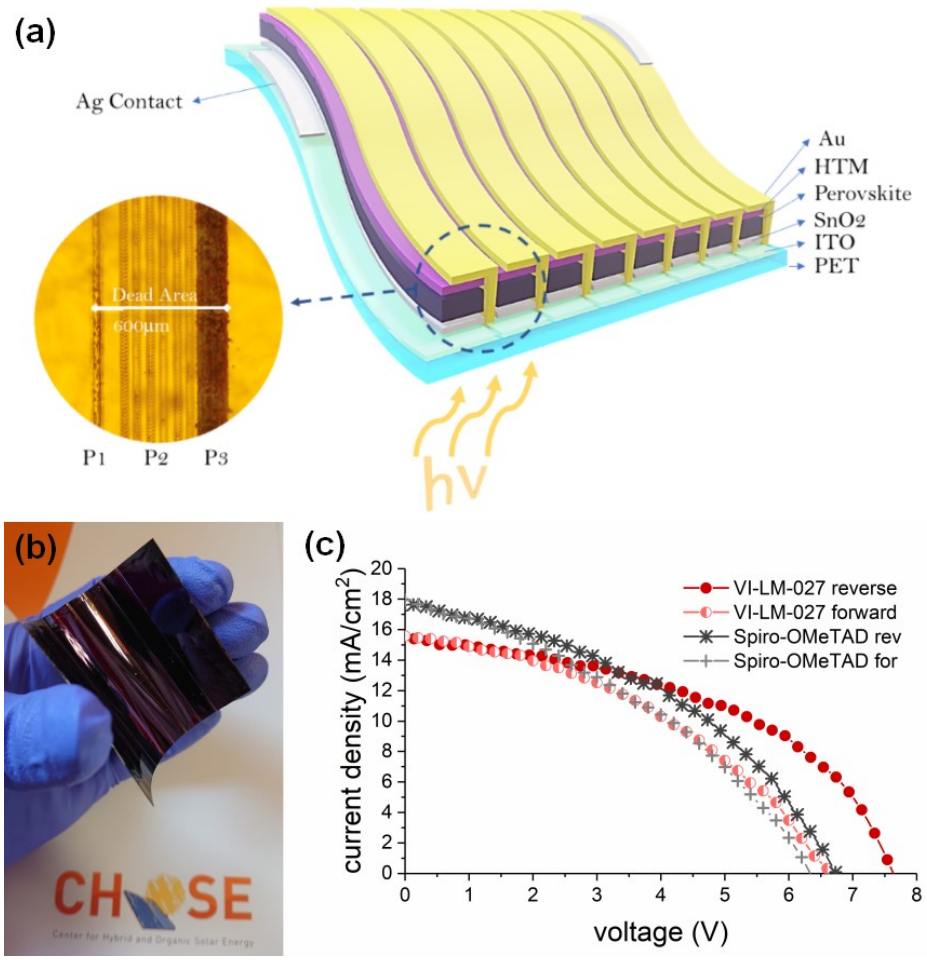


Figure 6. Flexible perovskite modules: (a) schematics of the flexible module, highlighting the layers, and microscope image of the interconnection area between adjacent cells with the P1, P2 and P3 scribes obtained by laser; the dead (non-active) area is about 600 nm wide, resulting in 87% aperture area; (b) photograph of one of the flexible modules fabricated for this work; (c) J-V curves in both reverse and forward scan directions for the best flexible modules employing spiro-OMeTAD and VI-LM-027 respectively as HTMs, showing comparable performance.

## 4. Conclusion

We synthetized BDT-modified P3HT polymers employing two different synthetic approaches, namely Stille and Kumada coupling. The former allows to control the amount of BDT inserted in the P3HT backbone, the latter to obtain relatively high molecular weight. Based on literature, three different HTMs, having a BDT/HT ratio equal to 1:2, 1:4 and 1:6, were synthetized by Stille coupling leading to relatively low molecular weight. On the other hand, Kumada's reaction allowed to obtain a polymer with MW close to 50 KDa, coded **VI-**

**LM-027**. Unfortunately, for the latter was not possible to exactly determinate the BDT:3HT ratio, but a reliable estimation is 1:35. Once implemented as HTMs in flexible perovskite, **VI-LM-027** showed efficiency comparable to commercial P3HT (MW = 94 kDa) and just slightly lower than spiro-OMeTAD. On the other hand, polymers synthetized by Stille coupling lead to relatively low efficiency, mainly related to insufficient fill factor, ascribable in turn to lower MW. More interestingly, **VI-LM-027** showed better stability than both spiro-OMeTAD and P3HT-94: upon light-soaked, it retained 90%, 60% and 30% of its initial efficiency after 1, 6 and 16 hours respectively, proving to be relatively more stable than the commercially available HTMs used as references; indeed, spiro-OMeTAD and P3HT-94 lost 80% of their initial performances after just 1 and 8 hours, respectively. Finally, to prove the scalability of the proposed materials, flexible PSK modules, made of 8 series-connected cells on a 6x6 $cm^2$ substrate, were fabricated and tested. The module endowed with **VI-LM-02**7as the HTM delivered a PCE close to 7% on an active area of 16 $cm^2$.

**Acknowledgements**

The authors would like to acknowledge the Italian Space Agency (ASI) for funding the PEROSKY project.

FDR, BT, FB would like to acknowledge the European Union's Horizon 2020 Research and Innovation Programme under grant agreement No763989 APOLO. This publication reflects only the author's views and the European Union is not liable for any use that may be made of the information contained therein.

NYN, ADC and CB would like to acknowledge the support of the Italian Ministry of Economic Development in the framework of the Operating Agreement with ENEA for Research on the Electric System.

The authors greatly acknowledge Luigi Angelo Castriotta (at CHOSE, Department of Electronic Engineering, Università degli Studi di Roma Tor Vergata) for laser scribing training and fruitful discussion. The authors acknowledge Prof. Pierluigi Quagliotto (at Department of Chemistry, University of Turin) for his wise advises during the synthesis of HTMs.

**Contribution of the authors** :

**FDR:** Conceptualization, Methodology, Investigation, Formal analysis, Visualization, Validation, Writing – Original Draft, Writing – Review & Editing

**GR:** Conceptualization, Methodology, Investigation, Formal analysis, Visualization, Validation, Writing – Original Draft, Writing – Review & Editing

**BT:** Investigation, Methodology, Formal analysis, Visualization, Validation, Writing – Original Draft, Writing – Review & Editing

**NYN:** Methodology, Validation, Investigation, Writing - Review & Editing

**VI:** Investigation, Methodology, Visualization, Validation

**AF:** Supervision, Writing – Review & Editing

**ADC:** Conceptualization, Supervision, Resources, Writing – Review & Editing

**MB:** Conceptualization, Methodology, Investigation, Formal analysis, Visualization, Validation, Writing – Original Draft, Writing – Review & Editing

**CB:** Conceptualization, Supervision, Resources, Project Administration, Funding Acquisition, Writing – Review & Editing

**FB:** Conceptualization, Supervision, Resources, Project Administration, Funding Acquisition, Writing – Review & Editing

## References


[1] K. Huang, Y. Peng, Y. Gao, J. Shi, H. Li, X. Mo, H. Huang, Y. Gao, L. Ding, J. Yang, High-Performance Flexible Perovskite Solar Cells via Precise Control of Electron Transport Layer, Adv. Energy Mater. 9 (2019) 1901419. doi:10.1002/aenm.201901419.

[2] NREL, Best Research-Cell Efficiency Chart | Photovoltaic Research | NREL, Best Res. Effic. Chart | Photovolt. Res. | NREL. (2019) https://www.nrel.gov/pv/cell-efficiency.html.

[3] M. Kaltenbrunner, G. Adam, E.D. Głowacki, M. Drack, R. Schwödiauer, L. Leonat, D.H. Apaydin, H. Groiss, M.C. Scharber, M.S. White, N.S. Sariciftci, S. Bauer, Flexible high power-per-weight perovskite solar cells with chromium oxide-metal contacts for improved stability in air, Nat. Mater. 14 (2015) 1032–1039. doi:10.1038/nmat4388.

[4] J. Zhang, W. Zhang, H.M. Cheng, S.R.P. Silva, Critical review of recent progress of flexible perovskite solar cells, Mater. Today. (2020). doi:10.1016/j.mattod.2020.05.002.

[5] Y. Rong, L. Liu, A. Mei, X. Li, H. Han, Beyond Efficiency: the Challenge of Stability in Mesoscopic Perovskite Solar Cells, Adv. Energy Mater. 5 (2015) n/a-n/a. doi:10.1002/aenm.201501066.

[6] E.H. Jung, N.J. Jeon, E.Y. Park, C.S. Moon, T.J. Shin, T.Y. Yang, J.H. Noh, J. Seo, Efficient, stable and scalable perovskite solar cells using poly(3-hexylthiophene), Nature. 567 (2019) 511–515. doi:10.1038/s41586-019-1036-3.

[7] T. Malinauskas, D. Tomkute-Luksiene, R. Sens, M. Daskeviciene, R. Send, H. Wonneberger, V. Jankauskas, I. Bruder, V. Getautis, Enhancing Thermal Stability and Lifetime of Solid-State Dye-Sensitized Solar Cells via Molecular Engineering of the Hole-Transporting Material Spiro-OMeTAD, ACS Appl. Mater. Interfaces. 7 (2015) 11107–11116. doi:10.1021/am5090385.

[8] T. Qin, W. Huang, J.E. Kim, D. Vak, C. Forsyth, C.R. McNeill, Y.B. Cheng, Amorphous hole-transporting layer in slot-die coated perovskite solar cells, Nano Energy. 31 (2017) 210–217.

doi:10.1016/j.nanoen.2016.11.022.

[9] F. Isabelli, F. Di Giacomo, H. Gorter, F. Brunetti, P. Groen, R. Andriessen, Y. Galagan, Solvent Systems for Industrial-Scale Processing of Spiro-OMeTAD Hole Transport Layer in Perovskite Solar Sells, ACS Appl. Energy Mater. 1 (2018) 6056–6063. doi:10.1021/acsaem.8b01122.

[10] K. Hwang, Y.-S. Jung, Y.-J. Heo, F.H. Scholes, S.E. Watkins, J. Subbiah, D.J. Jones, D.-Y. Kim, D. Vak, Toward large scale roll-to-roll production of fully printed perovskite solar cells., Adv. Mater. 27 (2015) 1241–7. doi:10.1002/adma.201404598.

[11] G. Saianand, P. Sonar, G.J. Wilson, A.I. Gopalan, V.A.L. Roy, G.E. Unni, K. Mamun Reza, B. Bahrami, K. Venkatramanan, Q. Qiao, Current advancements on charge selective contact interfacial layers and electrodes in flexible hybrid perovskite photovoltaics, J. Energy Chem. 54 (2021) 151–173. doi:10.1016/j.jechem.2020.05.050.

[12] Y. Zhao, Q. Ye, Z. Chu, F. Gao, X. Zhang, J. You, Recent Progress in High-efficiency Planar-structure Perovskite Solar Cells, ENERGY Environ. Mater. 2 (2019) 93–106. doi:10.1002/eem2.12042.

[13] Z. Bagheri, F. Matteocci, E. Lamanna, D. Di Girolamo, A.G. Marrani, R. Zanoni, A. Di Carlo, A. Moshaii, Light-induced improvement of dopant-free PTAA on performance of inverted perovskite solar cells, Sol. Energy Mater. Sol. Cells. 215 (2020) 110606. doi:10.1016/j.solmat.2020.110606.

[14] R.D. McCullough, The chemistry of conducting polythiophenes, Adv. Mater. 10 (1998) 93–116. doi:10.1002/(SICI)1521-4095(199801)10:2<93::AID-ADMA93>3.0.CO;2-F.

[15] M. Ates, T. Karazehir, A. Sezai Sarac, Conducting Polymers and their Applications, Curr. Phys. Chem. 2 (2012) 224–240. doi:10.2174/1877946811202030224.

[16] M. Zhang, M. Lyu, H. Yu, J.H. Yun, Q. Wang, L. Wang, Stable and low-cost mesoscopic CH3NH3PbI2Br perovskite solar cells by using a thin poly(3-hexylthiophene) layer as a hole

transporter, Chem. - A Eur. J. 21 (2015) 434–439. doi:10.1002/chem.201404427.

[17] A.T. Kleinschmidt, S.E. Root, D.J. Lipomi, Poly(3-hexylthiophene) (P3HT): Fruit fly or outlier in organic solar cell research?, J. Mater. Chem. A. 5 (2017) 11396–11400. doi:10.1039/c6ta08317j.

[18] Y. Yang, Y. Liu, Z. Hong, Q. Chen, H. Chen, W.H. Chang, T. Bin Song, Perovskite Solar Cells Employing Dopant-Free Organic Hole Transport Materials with Tunable Energy Levels, Adv. Mater. 28 (2016) 440–446. doi:10.1002/adma.201504293.

[19] Y. Miyazawa, M. Ikegami, H.W. Chen, T. Ohshima, M. Imaizumi, K. Hirose, T. Miyasaka, Tolerance of Perovskite Solar Cell to High-Energy Particle Irradiations in Space Environment, IScience. 2 (2018) 148–155. doi:10.1016/j.isci.2018.03.020.

[20] Z. Zhang, L. Qu, G. Shi, Fabrication of highly hydrophobic surfaces of conductive polythiophene, J. Mater. Chem. 13 (2003) 2858–2860. doi:10.1039/b309291g.

[21] N. Yaghoobi Nia, E. Lamanna, M. Zendehdel, A.L. Palma, F. Zurlo, L.A. Castriotta, A. Di Carlo, Doping Strategy for Efficient and Stable Triple Cation Hybrid Perovskite Solar Cells and Module Based on Poly(3-hexylthiophene) Hole Transport Layer, Small. (2019) 1904399. doi:10.1002/smll.201904399.

[22] Q. Hu, E. Rezaee, M. Li, Q. Chen, C. Li, S. Cai, H. Shan, Z.X. Xu, P3HT with Zn(C6F5)2 as p-Type Dopant for the Enhanced Performance of Planar Perovskite Solar Cells, Sol. RRL. 4 (2020) 1900340. doi:10.1002/solr.201900340.

[23] J.W. Jung, J.S. Park, I.K. Han, Y. Lee, C. Park, W. Kwon, M. Park, Flexible and highly efficient perovskite solar cells with a large active area incorporating cobalt-doped poly(3-hexylthiophene) for enhanced open-circuit voltage, J. Mater. Chem. A. 5 (2017) 12158–12167. doi:10.1039/c7ta03541a.

[24] P. Quagliotto, A. Fin, Advances in Synthetic Methods for the Preparation of Poly(3-

hexylthiophene) (P3HT), Lett. Org. Chem. 15 (2018) 991–1006. doi:10.2174/1570178615666180322150512.

[25] J. You, L. Meng, T.-B.T. Bin Song, T.F.T.-F. Guo, W.H.W.-H. Chang, Z. Hong, H. Chen, H. Zhou, Q. Chen, Y. Liu, N. De Marco, Y. Yang, Improved air stability of perovskite solar cells via solution-processed metal oxide transport layers, Nat. Nanotechnol. 11 (2016) 75–81. doi:10.1038/nnano.2015.230.

[26] Q.A. Yousif, S. Agbolaghi, A Comparison Between Functions of Carbon Nanotube and Reduced Graphene Oxide and Respective Ameliorated Derivatives in Perovskite Solar Cells, Macromol. Res. 28 (2020) 425–432. doi:10.1007/s13233-020-8054-8.

[27] J. Hynynen, D. Kiefer, L. Yu, R. Kroon, R. Munir, A. Amassian, M. Kemerink, C. Müller, Enhanced Electrical Conductivity of Molecularly p-Doped Poly(3-hexylthiophene) through Understanding the Correlation with Solid-State Order, Macromolecules. 50 (2017) 8140–8148. doi:10.1021/acs.macromol.7b00968.

[28] F. Di Giacomo, S. Razza, F. Matteocci, A. D'Epifanio, S. Licoccia, T.M. Brown, A. Di Carlo, High efficiency CH3NH3PbI(3-x)Cl x perovskite solar cells with poly(3-hexylthiophene) hole transport layer, J. Power Sources. 251 (2014) 152–156. doi:10.1016/j.jpowsour.2013.11.053.

[29] A.A. El-Shehawy, N.I. Abdo, A.A. El-Barbary, J.-S. Lee, Alternating Copolymers Based on 2,1,3-Benzothiadiazole and Hexylthiophene: Positioning Effect of Hexyl Chains on the Photophysical and Electrochemical Properties, European J. Org. Chem. 2011 (2011) n/a-n/a. doi:10.1002/ejoc.201100182.

[30] Y. Yuan, J. Huang, Ion Migration in Organometal Trihalide Perovskite and Its Impact on Photovoltaic Efficiency and Stability, Acc. Chem. Res. 49 (2016) 286–293. doi:10.1021/acs.accounts.5b00420.

[31] H. Usta, A. Facchetti, T.J. Marks, N-channel semiconductor materials design for organic

complementary circuits, Acc. Chem. Res. 44 (2011) 501–510. doi:10.1021/ar200006r.

[32] A. Kiriy, V. Senkovskyy, M. Sommer, Kumada catalyst-transfer polycondensation: Mechanism, opportunities, and challenges, Macromol. Rapid Commun. 32 (2011) 1503–1517. doi:10.1002/marc.201100316.

[33] N.Y. Nia, F. Matteocci, L. Cina, A. Di Carlo, A. Di Carlo, A. Di Carlo, High-Efficiency Perovskite Solar Cell Based on Poly(3-Hexylthiophene): Influence of Molecular Weight and Mesoscopic Scaffold Layer, ChemSusChem. 10 (2017) 3854–3860. doi:10.1002/cssc.201700635.

[34] R. Zhang, B. Li, M.C. Iovu, M. Jeffries-El, G. Sauvé, J. Cooper, S. Jia, S. Tristram-Nagle, D.M. Smilgies, D.N. Lambeth, R.D. McCullough, T. Kowalewski, Nanostructure dependence of field-effect mobility in regioregular poly(3-hexylthiophene) thin film field effect transistors, J. Am. Chem. Soc. 128 (2006) 3480–3481. doi:10.1021/ja055192i.

[35] A.O. Sunday, B.A. Alafara, O.G. Oladele, Toxicity and speciation analysis of organotin compounds, Chem. Speciat. Bioavailab. 24 (2012) 216–226. doi:10.3184/095422912X13491962881734.

[36] H.B. Stoner, J.M. Barnes, J.I. Duff, Studies on the toxicity of alkyl tin compounds., Br. J. Pharmacol. Chemother. 10 (1955) 16–25. doi:10.1111/j.1476-5381.1955.tb00053.x.

[37] Y. Gong, L. Xia, J. Song, Q. Liang, Synthesis of poly(3-hexylthiophene) with high molecular weight and small polydispersity, Adv. Mater. Res. 616–618 (2013) 1693–1696. doi:10.4028/www.scientific.net/AMR.616-618.1693.

[38] K. Matsubara, S. Miyazaki, Y. Koga, Y. Nibu, T. Hashimura, T. Matsumoto, An unsaturated nickel(0) NHC catalyst: Facile preparation and structure of Ni(0)(NHC)2, featuring a reduction process from Ni(II)(NHC)(acac) 2, Organometallics. 27 (2008) 6020–6024. doi:10.1021/om800488x.

[39] X. Shi, A. Sui, Y. Wang, Y. Li, Y. Geng, F. Wang, Controlled synthesis of high molecular weight

poly(3-hexylthiophene)s via Kumada catalyst transfer polycondensation with Ni(IPr)(acac)2 as the catalyst, Chem. Commun. 51 (2015) 2138–2140. doi:10.1039/c4cc08012b.

[40] T. Sudyoadsuk, P. Chasing, T. Kaewpuang, T. Manyum, C. Chaiwai, S. Namuangruk, V. Promarak, High efficiency and low efficiency roll-off hole-transporting layer-free solution-processed fluorescent NIR-OLEDs based on oligothiophene-benzothiadiazole derivatives, J. Mater. Chem. C. 8 (2020) 5045–5050. doi:10.1039/d0tc00450b.

[41] S. Li, X. Yang, L. Zhang, J. An, B. Cai, X. Wang, Effect of fluorine substituents on benzothiadiazole-based D-π-A′-π-A photosensitizers for dye-sensitized solar cells, RSC Adv. 10 (2020) 9203–9209. doi:10.1039/c9ra09693k.

[42] J. Yuan, Y. Zhang, L. Zhou, C. Zhang, T. Lau, G. Zhang, X. Lu, H. Yip, S.K. So, S. Beaupré, M. Mainville, P.A. Johnson, M. Leclerc, H. Chen, H. Peng, Y. Li, Y. Zou, Fused Benzothiadiazole: A Building Block for n-Type Organic Acceptor to Achieve High-Performance Organic Solar Cells, Adv. Mater. 31 (2019) 1807577. doi:10.1002/adma.201807577.

[43] I.B. Kim, D. Khim, S.Y. Jang, J. Kim, B.K. Yu, Y.A. Kim, D.Y. Kim, D-A copolymer with high ambipolar mobilities based on dithienothiophene and diketopyrrolopyrrole for polymer solar cells and organic field-effect transistors, Org. Electron. 26 (2015) 251–259. doi:10.1016/j.orgel.2015.07.003.

[44] T.A. Chen, X. Wu, R.D. Rieke, Regiocontrolled Synthesis of Poly(3-alkylthiophenes) Mediated by Rieke Zinc: Their Characterization and Solid-State Properties, J. Am. Chem. Soc. 117 (1995) 233–244. doi:10.1021/ja00106a027.

[45] R.D. Mccullough, R.D. Lowe, M. Jayaraman, D.L. Anderson, Design, Synthesis, and Control of Conducting Polymer Architectures: Structurally Homogeneous Poly(3-alkylthiophenes), 1993.

[46] M. Trznadel, A. Pron, M. Zagorska, R. Chrzaszcz, J. Pielichowski, Effect of molecular weight on spectroscopic and spectroelectrochemical properties of regioregular poly(3-hexylthiophene),

Macromolecules. 31 (1998) 5051–5058. doi:10.1021/ma970627a.

[47] S.L. Pittelli, S.A. Gregory, J.F. Ponder, S.K. Yee, J.R. Reynolds, Inducing planarity in redox-active conjugated polymers with solubilizing 3,6-dialkoxy-thieno[3,2-b]thiophenes (DOTTs) for redox and solid-state conductivity applications, J. Mater. Chem. C. 8 (2020) 7463–7475. doi:10.1039/d0tc00914h.

[48] B. Taheri, E. Calabrò, F. Matteocci, D. Di Girolamo, G. Cardone, A. Liscio, A. Di Carlo, F. Brunetti, Automated Scalable Spray Coating of SnO2 for the Fabrication of Low-Temperature Perovskite Solar Cells and Modules, Energy Technol. 8 (2020) 1901284. doi:10.1002/ente.201901284.

[49] J.P. Heiskanen, P. Vivo, N.M. Saari, T.I. Hukka, T. Kastinen, K. Kaunisto, H.J. Lemmetyinen, O.E.O. Hormi, Synthesis of Benzothiadiazole Derivatives by Applying C-C Cross-Couplings, J. Org. Chem. 81 (2016) 1535–1546. doi:10.1021/acs.joc.5b02689.